

# Simulation-Based Hanging Wall Effects

Jennifer L. Donahue<sup>a)</sup> M.EERI, and Norman A. Abrahamson<sup>b)</sup> M.EERI

The hanging wall (HW) effect is defined as the increase in ground motion at short distances for sites on the hanging wall side of a rupture when compared to sites on the footwall (FW) side at the same closest distance. In general, it is a geometrical effect due to the use of a closest distance metric, such as rupture distance, that does not capture the main features of the ground motion scaling for sites near dipping faults. To constrain the HW scaling on magnitude, distance, dip, and depth to top of rupture, finite-fault simulations were used to generate ground motions from 34 source geometries with 30 realizations of the slip distribution and hypocenter locations. The scaling of resulting response spectral accelerations at over 130,000 source/site combinations were parameterized to model the dependence of the HW effects. This HW scaling was utilized to constrain some of the NGA-West2 ground motion prediction equations. [DOI: 10.1193/071113EQS200M]

## INTRODUCTION

Following the 1994 Northridge, California, earthquake, [Abrahamson and Somerville \(1996\)](#) found that recorded ground motions on the hanging wall side of the fault were, on average, greater than ground motions at the same rupture distance on the footwall side. Using the available empirical data, they derived an empirical model for the HW effect which results in a 50% increase in peak horizontal accelerations over the hanging wall, which attenuated with distance. From these findings, they postulated that high-frequency ground motions for other reverse events would lead to similar systematic increases. Later, the near fault data from the 1999 Chi-Chi earthquake also showed a systematic increase in the short period ground motions on the HW side of the fault compared to the ground motions on the FW side at the same rupture distance. The near-fault ground motions from the Chi-Chi earthquake showed stronger HW effects than observed in the Northridge earthquake, with an increase of a factor of 2 to 3 for short periods. The recordings from these two earthquakes showed that the HW effect can be an important factor for estimation of near-fault ground motions near dipping faults.

The HW effect is due to the shortcomings of the rupture distance metric for sites located close to large dipping faults. The HW effect is primarily a geometrical effect that is well known for empirical GMPEs. Consider two sites at the same rupture distance, but with one site on the FW and one site in the HW. The site located over the HW will be closer to more of the rupture than the site located on the FW. The expected HW factor due simply to geometry can be evaluated using the root mean square of  $1/(R_{RUP} + 1)$  averaged over the rupture plane as a proxy for the contribution from different parts of the rupture down dip.

---

<sup>a)</sup> Geosyntec Consultants, 595 Market Street, San Francisco, CA 94105

<sup>b)</sup> Pacific Gas & Electric Company, 245 Market Street, San Francisco, CA 94105

For the geometry shown in the lower frame of Figure 1, the natural log of  $RMS(1/(R_{RUP} + 1))$  for sites on the FW was fit to a simple parametric form and the resulting model was used to compute the residuals for both FW and HW sites. The residuals, shown in the upper frame of Figure 1, reach a maximum over the bottom edge of the rupture. For this case, the rupture distance metric is not able to capture the differences in the path effects for the FW and HW sites. In contrast, the  $R_{JB}$  distance metric does distinguish between these two sites because it is based on the horizontal distance to the surface projection of the rupture.

In 2008, the Next Generation Attenuation (NGA) project, coordinated by the Pacific Earthquake Engineering Research Center (PEER), developed five ground motion prediction equations (GMPEs). Three of these models—[Abrahamson and Silva \(2008; AS08\)](#), [Campbell and Bozorgnia \(2008; CB08\)](#), and [Chiou and Youngs \(2008; CY08\)](#)—explicitly incorporated the hanging wall (HW) effect in their ground motion prediction equation (GMPE). The [Boore and Atkinson model \(2008; BA08\)](#) did not specifically include a HW term, but the effect of the hanging wall is implicitly captured by the use of the  $R_{JB}$  distance as the primary distance metric. The [Idriss model \(2008; I08\)](#) did not address hanging wall effects.

Empirical data needed to constrain the hanging wall event is contingent on having a dataset with recordings on both the hanging wall and footwall sides of the rupture, at short distances. The earthquakes in the NGA (2008) dataset that can be used to constrain the HW scaling are listed in Table 1. Only two earthquakes in the 2008 dataset had more than one recording located over the rupture plane (1994 Northridge and 1999 Chi-Chi). Five other earthquakes (1980 Irpinia, 1987 Whittier Narrows, 1989 Loma Prieta,

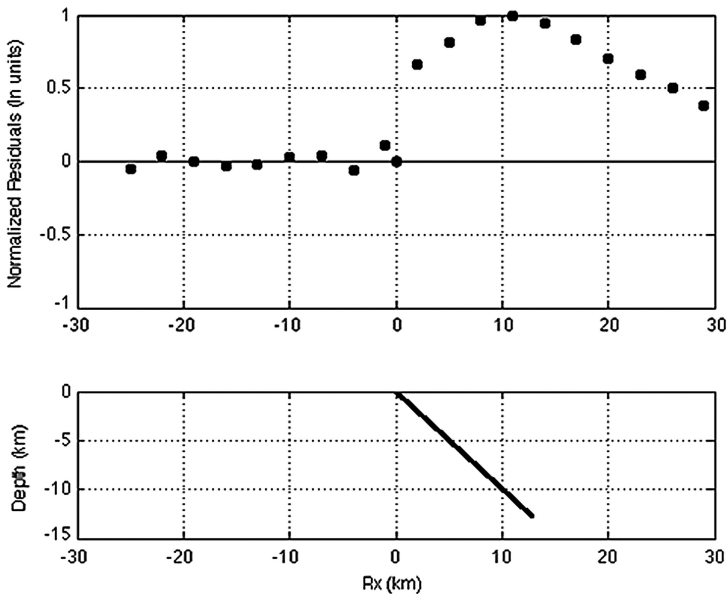


**Figure 1.** Example of expected distance dependence of the HW effects from a  $45^\circ$  dipping rupture due simply to geometrical effects. Residuals are normalized to a maximum of unity.

**Table 1.** List of earthquakes in the 2008 NGA and 2013 NGA-West2 databases with a dip less than or equal to  $70^\circ$ , at least five recordings within 80 km, and at least one recording on both the footwall and hanging wall with  $R_{JB}$  distances of 15 km or less, located along the rupture

Database	Event	Year	Mag	Dip	Rake	# of recs	# of recs $R_{JB} = 0$	# of recs <15 km on FW	# of recs <15 km on HW
NGA (2008)	Irpinia, Italy-01	1980	6.9	60	-90	5	0	1	1
NGA (2008)	Whittier Narrows-01	1987	5.99	30	150	13	1	5	6
NGA (2008)	Loma Prieta, CA	1989	6.93	70	140	14	1	3	6
NGA (2008)	Northridge-01	1994	6.69	40	103	26	10	3	12
NGA (2008)	Chi-Chi, Taiwan	1999	7.62	33	55	53	7	24	7
NGA (2008)	Chi-Chi, Taiwan-06	1999	6.3	30	100	34	1	2	1
NGA-W2	Niigata, Japan	2004	6.63	47	93	23	0	2	2
NGA-W2	L'Aquila, Italy	2009	6.3	48	-98	7	4	2	4
NGA-W2	Wenchuan, China	2008	7.9	50	138	34	3	1	5
NGA-W2	Iwate	2008	6.9	40	104	37	1	2	3
NGA-W2	El Mayor-Cucapah	2010	7.2	63	-164	9	0	1	1
NGA-W2	Christchurch, New Zealand	2011	6.2	67	135	6	1	4	2

1995 Kobe, 1999 Chi-Chi-06) had at least one recording located along the rupture (source-to-site azimuth of  $90^\circ$  or  $-90^\circ$ ) on both the FW and HW at an  $R_{JB}$  distance of less than 15 km. With only this limited data available, the developers of the 2008 NGA GMPEs had to make assumptions about the magnitude, dip, and  $Z_{TOR}$  scaling of the HW effects. These different assumptions, which were not well constrained, led to large differences in the HW effects between the different 2008 NGA GMPEs. For example, the AS08 model assumed that the HW effect was magnitude dependent with no effect below  $M$  6.0, whereas the CY08 model assumed the full HW effects applied to  $M$  6.0 earthquakes, leading to large differences in the predicted ground motions for sites over the HW for  $M$  6.0 earthquakes for these two models.

With the completion of the NGA-West2 database, several additional earthquakes that can help constrain the HW scaling were added (Table 1). Two additional earthquakes had multiple recordings over the rupture plane (2009 L'Aquila and 2008 Wenchuan) and five additional earthquakes had at least one recording on both the footwall and hanging wall with  $R_{JB}$  distances of 15 km or less. Event with this additional data, there is still not enough empirical data to provide robust constraints on the HW scaling. Therefore, we use one-dimensional finite-fault simulations to provide constraints on the HW scaling.

## FINITE FAULT SIMULATIONS

The [Graves and Pitarka \(2010\)](#) modules on the Southern California Earthquake Center (SCEC) broadband platform (BBP) are used for the simulations. The Graves and Pitarka (GP2010) methodology is a hybrid broadband methodology, in that it combines a

deterministic approach at low frequencies ( $f < 1$  Hz) with a stochastic approach at high frequencies ( $f > 1$  Hz). The fault rupture is represented kinematically and incorporates spatial heterogeneity in slip, rupture speed, and rise time. The focus of our evaluation is on the short-period range, which is controlled by the stochastic approach. The GP2010 method has been evaluated as part of the SCEC BBP validation project (Dreger et al. 2013), which compares simulated ground motions to recordings from seven past earthquakes and to ground motions from empirical GMPEs in the magnitude and distance ranges for which they are well constrained. The SCEC evaluation found that the GP2010 method passed the validation test for periods from 0 s to 3 s.

Using the GP2010 modules on the BBP, 34 reverse earthquake events (listed in the Supplemental Table S-1) were simulated. The scenarios varied the magnitude between **M** 6 and **M** 7.8, dips from  $20^\circ$  to  $70^\circ$ , and  $Z_{TOR}$  values of 0 km and 5 km. Each scenario was run 30 times, with randomized hypocenter locations (along-strike and down-dip) and slip distributions. An example of slip distribution is presented in Figure 2.

The one-dimensional (1-D) velocity model used in the simulations uses the GP2010 model developed for the Loma Prieta earthquake with values shown in the Table A2 in online Appendix A. This crustal model is for a soft-rock site with a shear-wave velocity over the top 30 m ( $V_{S30}$ ) of 865 m/s. The grid size for the source model was set to 400 m, which limits the useable bandwidth for the deterministic part of the simulation; however, for the stochastic part of the simulation, the GP2010 method averages the slip over  $1 \text{ km} \times 1 \text{ km}$  grid, so the 400 m grid size does not affect the useable frequency band for the high frequencies. To stay in the stochastic range, we only show the results for frequencies greater than 2 Hz.

Acceleration time histories were simulated along a grid on both sides of the fault rupture, with horizontal distances ranging from 1 km to 100 km. An example station map for one scenario is presented in Figure 3. Small magnitudes (**M** 6 and **M** 6.5) used 105 stations, while larger events ( $> \text{M}$  7) used up to 300 stations. In all, seismograms were simulated for about 130,000 source/site combinations. An example of the three-component accelerograms for one realization at a FW site and HW site is shown in Figure 4. This example shows that the increase in the HW accelerations is a broad increase and is not due to a single spike.

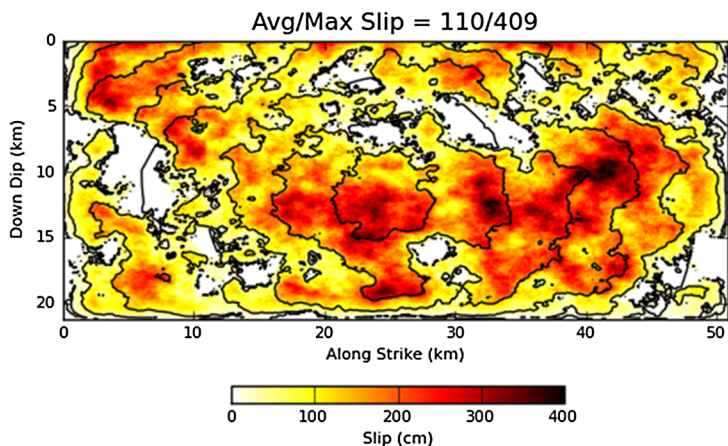


**Figure 2.** Example slip distribution for **M** 7 with a dip of  $45^\circ$ .

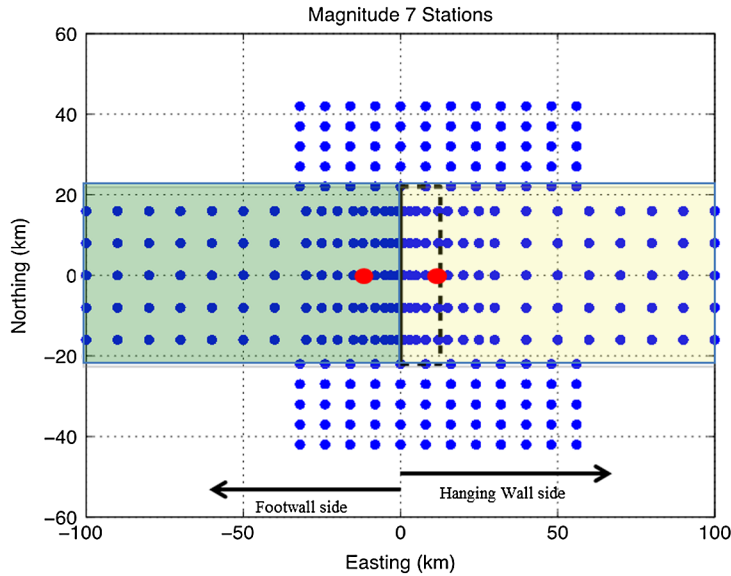


**Figure 3.** Station location map for  $M$  7 with a dip of  $45^\circ$ . Stations included in the footwall GMPE regression are shown in light green. Stations included in the regression of the hanging wall term are shown in light yellow. Example seismograms shown in Figure 3 are shown as stations in red above.

The simulations from the 34 earthquake scenarios led to a large dataset of ground motions at short distances on both the hanging wall and footwall sides of the rupture. To develop the model for the HW scaling, we first developed a simple GMPE for the ground motions on the footwall (FW) side of the rupture only so that we could remove the basic magnitude and distance scaling in the simulated data. Initially, a standard form of a GMPE, shown in Equation 1, was fit to the FW data:

$$\ln(SA) = b_1 + (b_2 + b_3 \times (\mathbf{M} - 6)) \times (\ln((R_{RUP}) + b_4)) + b_5 \times (\mathbf{M} - 6) + b_6 \times (\mathbf{M} - 6)^2 + b_7 \times (R_{RUP}) \quad (1)$$

The initial exploratory analysis showed that the simulated data had a strong dependence on the dip and  $Z_{TOR}$ . To remove this dip and  $Z_{TOR}$  dependence from the FW ground motions, the simple form was modified to include a dip and  $Z_{TOR}$  dependence shown in Equation 2:

$$\ln(SA) = b_1 + (b_2 + b_3 \times (\mathbf{M} - 6)) \times (\ln((R_{RUP}) + b_4)) + b_5 \times (\mathbf{M} - 6) + b_6 \times (\mathbf{M} - 6)^2 + b_7 \times (R_{RUP}) + f_{dip}(\delta) + f_{ZTORFW}(Z_{TOR}, \delta, \mathbf{M}) \quad (2)$$

where:

$$f_{dip}(\delta) = d_1 \times (90 - \delta)^2 + d_2 \times (90 - \delta) + d_3 \quad (3)$$

$$f_{ZTORFW}(Z_{TOR}, \delta, \mathbf{M}) = (z_{f11} \times (90 - \delta) + z_{f12}) + (z_{f13} \times (\mathbf{M} - 6)) \quad (4)$$

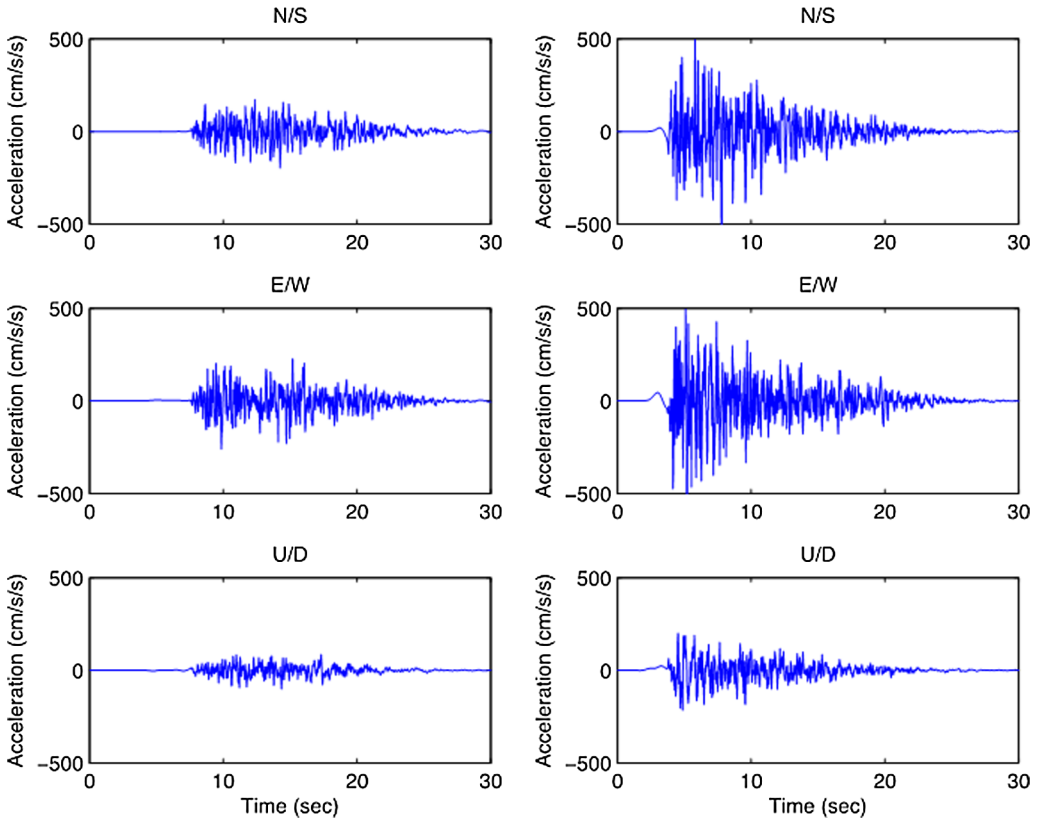


**Figure 4.** Example seismograms for a  $M 7$  with a dip of  $45^\circ$  at on the footwall at  $R_x = -12$  km (left hand panels) and on the hanging wall at  $R_x = 12$  km (right hand panels). Station locations are shown in Figure 2 above.

and  $SA$  is the spectral acceleration (in  $g$ ),  $M$  is the moment magnitude,  $R_{RUP}$  is the closest distance from the rupture to the site in km,  $\delta$  is the dip of the rupture plane,  $Z_{TOR}$  is the depth to the top of rupture in km.

Using this modified form led to an adequate fit for the median ground motion on the footwall side of the fault. As an example, the residuals of the FW ground motions for a spectral period of  $T = 0.2$  s are shown as a function of magnitude,  $R_x$ , dip, and  $Z_{TOR}$ , in Figure 5.

### HANGING WALL MODEL DEVELOPMENT

To develop the model for the HW effects, the ground motions on the HW are first compared to the footwall GMPE (Equation 2). As an example, Figure 6 compares the  $T = 0.2$  s spectral accelerations on the FW and HW to the median spectral acceleration from the FW GMPE for a  $M 7.0$  surface rupturing earthquake with a dip of  $45^\circ$ . The short-period simulated

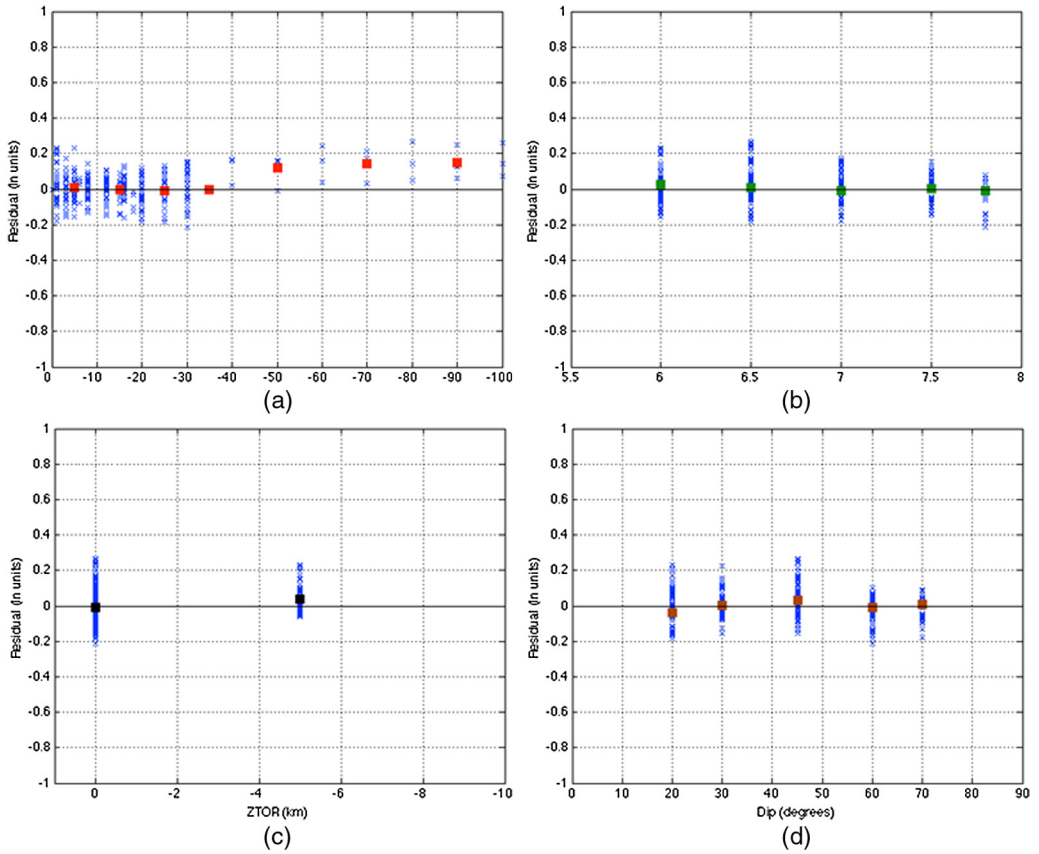


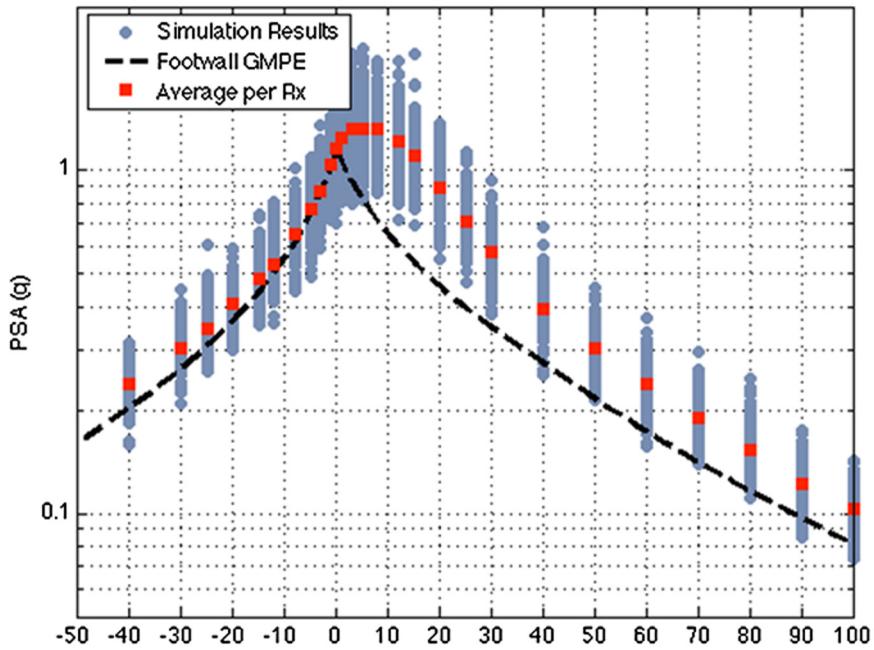
**Figure 5.** (a) Residuals (in natural log units) for magnitude; (b) residuals (in natural log units) for distance, in kilometers; (c) residuals (in natural log units) for the dip, in degrees; (d) residuals (in natural log units) for the top of rupture ( $Z_{TOR}$ ) in kilometers.

data on the HW are much larger than predicted by the FW GMPE. The mean residuals are also shown in Figure 6. For this scenario, the largest HW effect is about 0.7 natural log units (a factor of 2) and reaches its maximum near the point that is located over the bottom edge of the rupture, consistent with the simple geometrical effects discussed in the introduction.

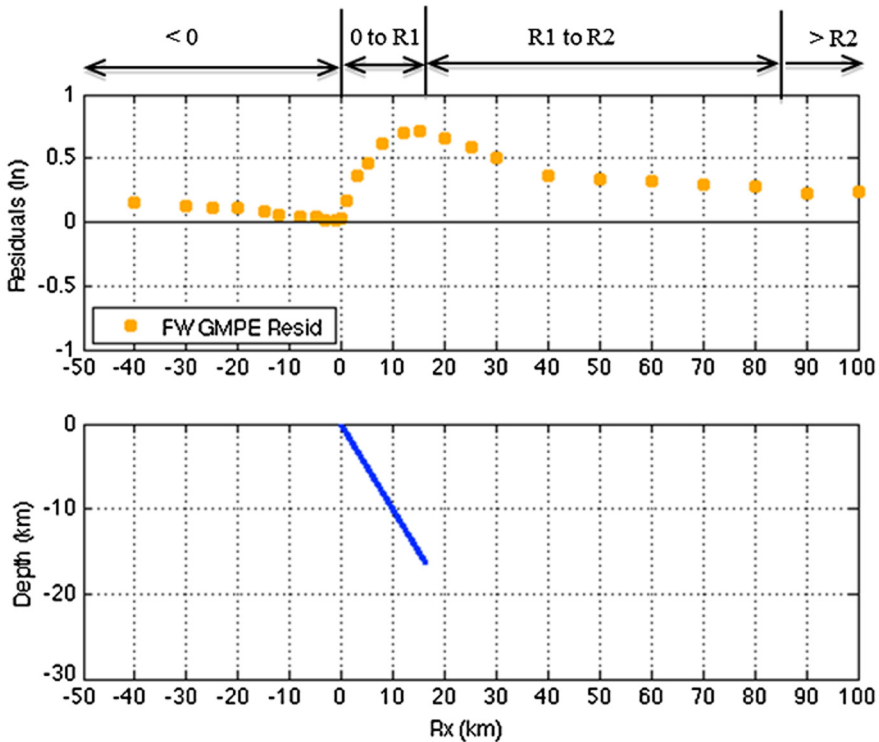
The HW residuals were computed for each of the 34 scenarios. Based on the trends in the residuals, a parametric model for the hanging wall effect was developed. The form of the HW effect model was set so that it could be easily incorporated into the forms of the GMPEs being used in the NGA-West2 project (Bozorgnia et al. 2014).

The hanging wall term is composed of an amplitude term ( $a_1$ ) and five scaling terms: dip, magnitude, distance perpendicular to the rupture, depth to top of rupture, and distance off the end of the rupture. The model of the HW effect,  $f_{hw}$ , is given by:

Magnitude 7, Dip = 45deg, Length = 44km, zTor = 0 km, Rake = 90 deg, Period = 0.2sec



(a)



(b)

**Figure 6.** (a) Application of the footwall GMPE (black dashed line) to the hanging wall side of the fault. Red squares are representative of the mean acceleration (in g's) for each  $R_x$  distance and (b) residuals (in natural log units, shown as the orange circles) of mean acceleration compared to the footwall GMPE.

$$f_{hw}(\mathbf{M}, \delta, W, Z_{TOR}, R_x, R_y, L) = a_1 T_1(\delta) T_2(\mathbf{M}) T_3(R_x, W, \delta, M) T_4(Z_{TOR}) T_5(R_x, R_y, L) \quad (5)$$

where  $\delta$  is the dip of the fault,  $R_x$  is the horizontal distance from the top of the rupture to the site measured perpendicular to strike ( $R_x$  is positive for sites on the HW side of the rupture and negative for site located on the FW side of the rupture),  $W$  is the down-dip rupture width,  $Z_{TOR}$  is the depth to top of rupture,  $R_y$  is the horizontal distance from the center of the rupture measured parallel to strike (see [Ancheta et al. 2013](#)), and  $L$  is the rupture length.

The amplitude term,  $a_1$ , is normalized and represents the HW effect for a  $\mathbf{M}$  6.5 surface-rupturing earthquake with a dip of  $45^\circ$  and for a site located over the bottom edge of the rupture. The distance scaling is separated into two parts:  $T_3$  captures the scaling with distance perpendicular to strike and  $T_5$  captures the scaling with distance off the edge of the rupture. The dip scaling also appears in two terms. The first term,  $T_1$ , captures the scaling with dip for all distances and third term,  $T_3$ , captures the dip dependence of the distance scaling. The terms in the HW effect are described below.

### DIP SCALING

The dip term,  $T_1$ , scales linearly with dip and is normalized to be unity for a fault with a  $45^\circ$  dip and takes the form as shown below:

$$T_1(\delta) = (90 - \delta)/45 \quad \text{for } \delta \leq 90^\circ \quad (6)$$

This model is applicable for dips of  $30^\circ$  or more, but, as will be shown later, the simulated data are not consistent with this model for dips less than  $30^\circ$ . It is currently not clear as to the cause for the change in scaling for dips less than  $30^\circ$  from the simulated data.

### MAGNITUDE SCALING

The magnitude term,  $T_2$ , scales linearly with magnitude and is normalized to unity for an event with  $\mathbf{M}$  6.5 and takes the form as shown below:

$$T_2(M) = 1 + a_2(\mathbf{M} - 6.5) \quad (7)$$

The smallest magnitude considered in the 34 scenarios is 6.0. The scaling from Equation 7 does not go to zero at  $\mathbf{M}$  6, therefore, the extrapolation of the magnitude scaling below  $\mathbf{M}$  6 is not constrained by these simulations and must be treated using other information and/or assumptions for use in a GMPE.

### DISTANCE SCALING

The first distance term,  $T_3$ , is dependent on the  $R_x$  distance and has four distance ranges: site located on the FW ( $R_x < 0$ ), sites located over the rupture plane ( $0 < R_x < R_1$ ), and two ranges for sites located off the rupture, as shown in Figure 5. The  $R_x$  value over the bottom edge of the rupture is denoted  $R_1$ . For sites located directly over the hanging wall, the distance function increases as the stations move away from the top of the rupture plane to the bottom edge of the rupture plane ( $f_1$  term; Equation 10). Using the  $f_1$  equation, the hanging wall effect reaches its maximum value over the bottom edge of the rupture. As the distance increases further from the rupture plane, the  $f_2$  term (Equation 11) is utilized until  $R_x$  is

greater than the  $R_2$  term (Equation 9). Using the  $f_2$  term, the hanging wall effect decreases parabolically with distance from the surface projection of the bottom edge of the rupture plane. At greater distances than  $R_2$ , the hanging wall effect decreases exponentially using the  $f_3$  term (Equation 13).

$$T_3(R_x, W, \delta, \mathbf{M}) = \begin{cases} 0 & \text{for } R_x < 0 \\ f_1(R_x, R_1) & \text{for } 0 < R_x \leq R_1 \\ f_2(R_x, R_1, R_2) & \text{for } R_1 < R_x \leq R_2 \\ f_3(R_x, R_2) & \text{for } R_x > R_2 \end{cases} \quad (8)$$

$$R_1(W, \delta) = W \cos(\delta) \quad (9)$$

$$R_2(\mathbf{M}) = 62 \mathbf{M} - 350 \quad (10)$$

where

$$f_1(R_x) = h_1 + h_2(R_x/R_1) + h_3(R_x/R_1)^2 \quad (11)$$

$$f_2(R_x) = h_4 + h_5((R_x - R_1)/(R_2 - R_1)) + h_6((R_x - R_1)/(R_2 - R_1))^2 \quad (12)$$

$$f_3(R_x, \mathbf{M}) = (h_4 + h_5 + h_6) \times \exp(-(R_x - R_y)\gamma) \quad (13)$$

where  $\gamma = -0.2\mathbf{M} + 1.65$ .

## DEPTH TO TOP OF RUPTURE SCALING

Only two values of  $Z_{TOR}$  were modeled: 0 km and 5 km. The amplitude of the HW effect for  $Z_{TOR} = 5$  km is 30% smaller than the HW effect for surface rupture, so there is a dependence on  $Z_{TOR}$ . However, with only two points, the form of the  $Z_{TOR}$  scaling is not constrained; it is not known if the scaling is linear between 0 km and 5 km, nor is it known how the  $Z_{TOR}$  scaling extrapolates to  $Z_{TOR}$  values greater than 5 km.

## RUPTURE EDGE DISTANCE SCALING

The second distances scaling,  $T_5$ , is a taper that is applied to sites located off the end of the rupture at source-to-site angles of  $45^\circ$  to  $90^\circ$  and from  $90^\circ$  to  $135^\circ$ . This taper allows for a gradual decrease in the HW effect at sites that are not within the length of the rupture (source-to-site angle of  $90^\circ$ ). This taper is parameterized by an additional distance metric,  $R_y$ . If  $R_y$  is greater than half the rupture length ( $L/2$ ), then the site is located off the end of the rupture. Therefore, the  $T_5$  term is set to unity for sites located along the rupture with  $R_y \leq L/2$ . The taper rupture edge scaling is shown in Figure 7.

$$T_5(R_x, R_y, L) = \begin{cases} 1 & \text{for } |R_y| \leq 0.5 L \\ \frac{0.577R_x + 5 - (|R_y| - 0.5 L)}{0.577R_x + 5} & \text{for } 0.5 L < |R_y| < 0.577R_x + 5 + 0.5 L \\ 0 & \text{for } |R_y| \geq 0.577R_x + 5 + 0.5 L \end{cases} \quad (14)$$

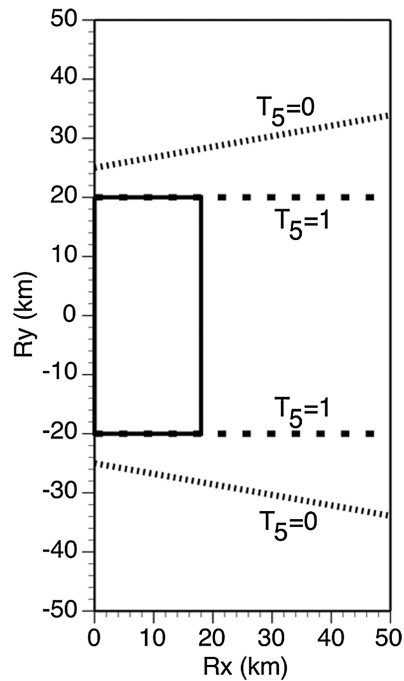


**Figure 7.** Example of the off-end of rupture taper term,  $T_5$ . The solid line shows the surface projection of the rupture plane.

This model leads to smooth tapering of the HW effects off the end of the rupture and represents an improvement over the [Abrahamson and Silva \(1997\)](#) model in which sites on the hanging wall side of the rupture with a source-to-site azimuth between  $45^\circ$  and  $135^\circ$  were given the full HW effect, whereas sites outside this range were given no HW effects. For the hanging wall model in the current study, only stations with a source-to-site azimuth of  $90^\circ$  are calculated with the full HW effect; for stations off the edge of the rupture the HW effect is tapered to zero as the azimuth decreases from  $90^\circ$  to  $45^\circ$  and likewise increases from  $90^\circ$  to  $135^\circ$ .

## RESULTS

The coefficients for the HW model (Equation 5) were estimated using ordinary least-squares. The coefficients vary smoothly with period and the coefficients for a representative set of periods are listed in Table A3 of online Appendix A. An example of the fits of the HW model to the simulated data is shown in Figures 8a and 8b.

The mean residuals by scenario are shown as a function of  $R_x$  in Figure B1 of online Appendix B. In each case, the residuals for all 30 realizations are averaged over all sites with the same  $R_x$  values. The mean residuals for sites on the hanging wall side of the rupture generally fall within the range  $-0.2$  to  $0.2$  natural log units with the exception of small magnitude events with shallow dipping faults: the **M** 6 and **M** 6.5 with shallow dips of  $20^\circ$  and

Magnitude 7, Dip = 45deg, Length = 44km, zTor = 0 km, Rake = 90 deg, Period = 0.2sec

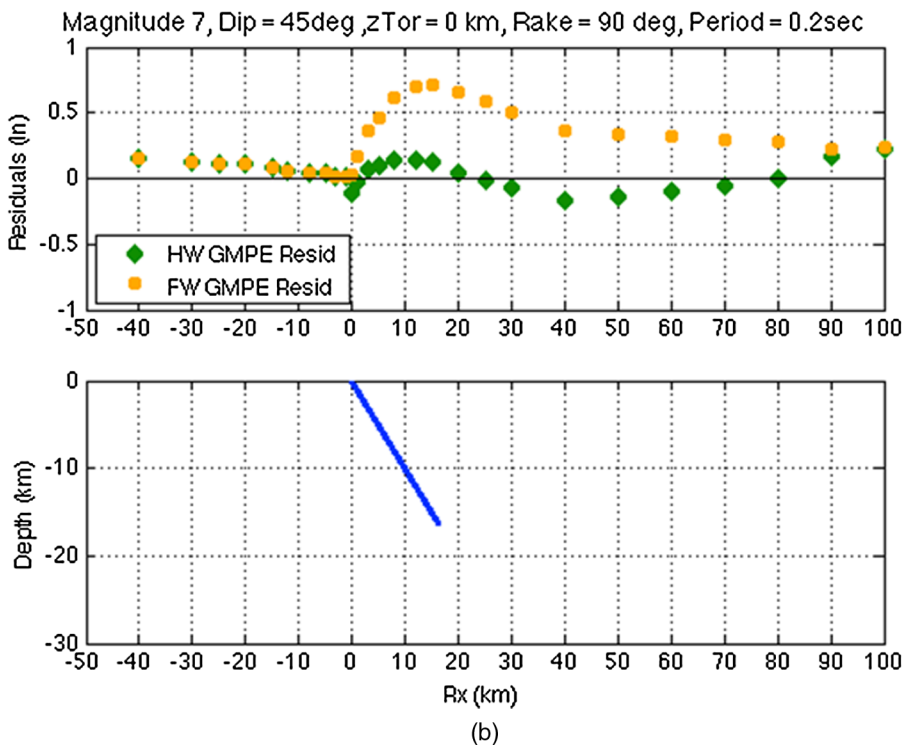
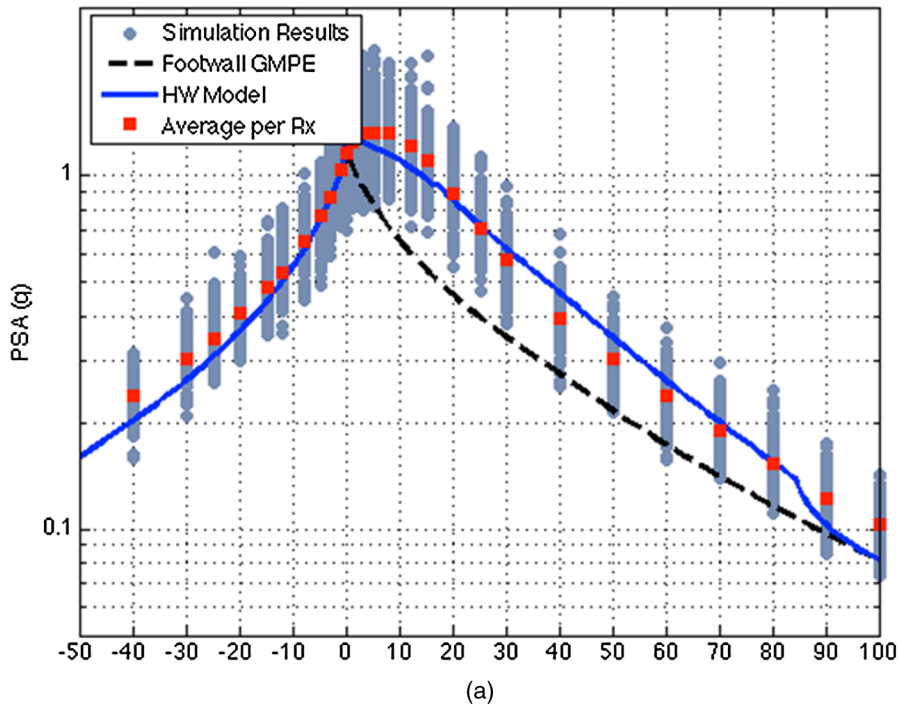


**Figure 8.** (a) Application of the hanging wall model (blue solid line to all stations along the fault) and (b) residuals from the footwall and hanging wall models.

30° and **M** 7 with a shallow dip of 20° show large negative residuals indicating the HW model is overpredicting the ground motion for these cases.

For buried ruptures,  $Z_{TOR} = 5$  km, these large negative residuals are not seen in the simulations for shallow dipping ruptures, suggesting that the differences are related to the increase of rise time for shallow slip in the top 5 km in the [Graves and Pitarka \(2010\)](#) method. The available empirical data for low dip angles and moderate magnitudes are from the 1980 Whittier Narrows earthquake and 1999 Chi-Chi-06 aftershock which are both buried ruptures, so they do not provide an empirical check on the scaling for shallow ruptures.

For sites located near the surface trace of the rupture ( $-1 \text{ km} < R_x < 1 \text{ km}$ ), the model tends to over-predict the ground motions for **M** 7.0–**M** 7.5, but this over-prediction at the top of the rupture is not seen for **M** 6.0–**M** 6.5 or for **M** 7.8. For the **M** 7.8 scenarios, the model over-predicts the HW effect at  $R_x$  distances greater than 10 km.

### COMPARISON TO EMPIRICAL DATA IN NGA-WEST2 DATABASE

Using the four events with more than one recording located over the hanging wall listed in [Table 1](#), the intra-event residuals from the [Abrahamson et al. \(2013\)](#) FW model were compared to the HW model from the simulations in [Figure 9](#). The HW term correlates well for the Northridge, Chi-Chi, and Wenchuan events; however, the HW ground motions for the L'Aquila earthquake are much larger over the bottom edge of the fault than predicted by the model.

### NGA-WEST2 GMPE COMPARISONS

The [Abrahamson et al. \(2013\)](#) and the [Campbell and Bozorgnia \(2013\)](#) GMPEs used parts of the simulation-based HW model to constrain the HW scaling for sites located over the surface projection of the rupture plane, but the amplitude of the scaling,  $a_1$ , was derived from the empirical data. The [Chiou and Youngs \(2013\)](#) GMPE does not use the HW model described within this paper, but instead relies on a hanging wall term that better fits with their base functional form. The [Boore et al. \(2013\)](#) GMPE does not specifically include a hanging wall term, but the effect of the hanging wall is implicitly captured by the use of the  $R_{JB}$  distance term. The [Idriss \(2013\)](#) GMPE does not include a hanging wall term, nor does it intend to capture differences between the ground motion on the FW and HW.

The HW scaling from the five models is compared to the HW scaling from the simulations in [Figures B2, B3, and B4](#) of online Appendix B. In each figure, the ground motion is normalized to the FW motion at an  $R_x$  distance of 12 km to remove differences in the GMPEs on the FW to isolate the hanging wall effect from the HW predictions. [Figure B2](#) compares the GMPEs for a range of magnitudes for a fixed dip of 45°; [Figure B3](#) compares the HW scaling for different dip angles for **M** 7 earthquakes; and [Figure B4](#) compares the HW scaling for different  $Z_{TOR}$  values. These comparison show that for sites located over the rupture plane, the GMPEs with HW effects tend to have larger HW factors than the HW model from the simulations, but the HW scaling simulations are similar to the  $R_{JB}$ -based BSSA model. At large distances ( $R_x > 20$  km), the simulations show a much weaker attenuation than all of the GMPEs. The objective of the simulations was to constrain the relative scaling

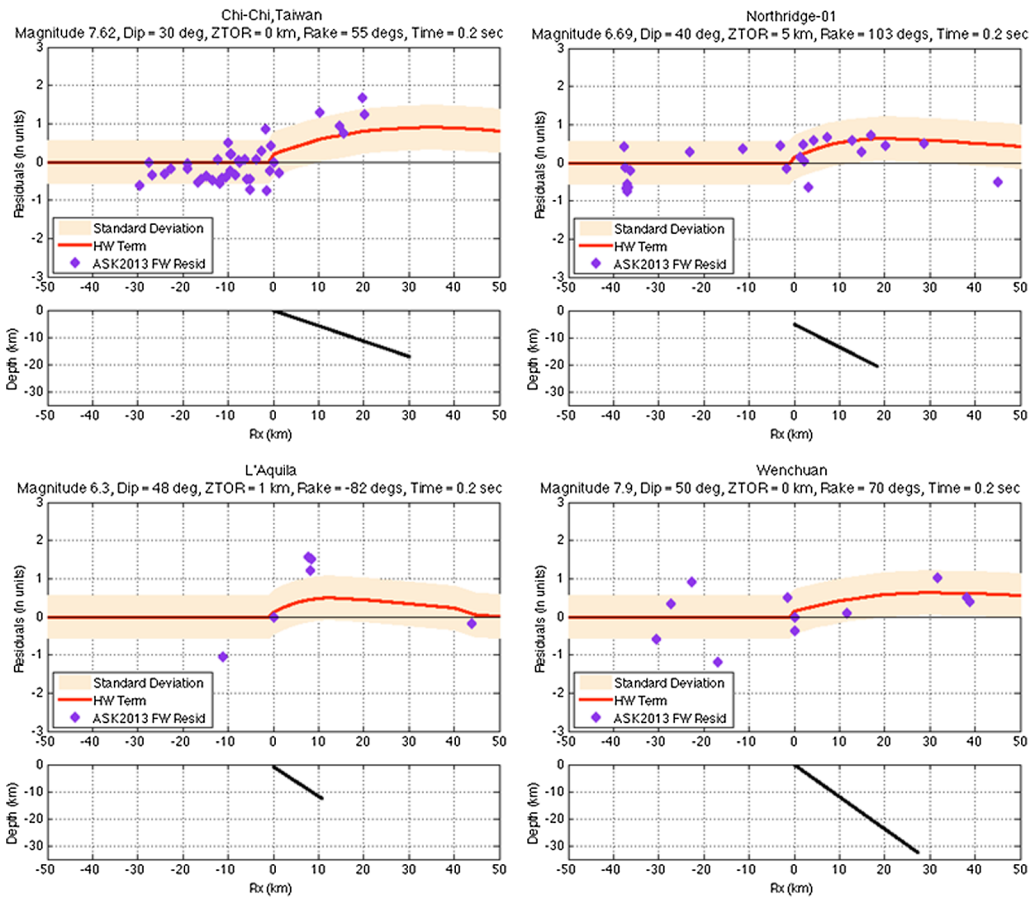


**Figure 9.** Intra-event residuals (in natural log units) for selected events with 3 or more recordings directly over the rupture plane: (upper left) Northridge, (upper right) Chi-Chi, (lower left) L'Aquila, (lower right) Wenchuan.

of the hanging wall effect while allowing the empirical data to constrain the overall amplitude of the hanging wall effect. We do not recommend using the HW model from the simulations directly for estimating ground motion amplitudes.

## CONCLUSIONS

The hanging wall model developed from the results of 1-D finite-fault simulations presented in the text and figures above provides a constraint on the scaling of hanging wall effects that can be used to constrain scaling of the GMPEs. The model provides a robust scaling of the HW effect on the ground motion at short distances for sources with dips between  $30^{\circ}$ – $90^{\circ}$  and magnitudes between 6 and 8. At greater distances away from the bottom edge of the hanging wall, the simulations results do not attenuate in similar fashion to the empirical data leading to a possible overprediction of the hanging wall effect at great distances.

## APPENDICES A AND B

To access the supplemental tables in Appendix A and the supplemental figures in Appendix B, please refer to the online edition of this paper.

## REFERENCES

- Abrahamson, N. A., and Silva, W., 1997. Empirical response spectral attenuation relations for shallow crustal earthquakes, *Seismological Research Letters* **68**, 94–127.
- Abrahamson, N. A., and Silva, W. J., 2008. Summary of the Abrahamson & Silva NGA ground motion relations, *Earthquake Spectra* **24**, 67–97.
- Abrahamson, N. A., Silva, W. J., and Kamai, R., 2013. *Update of the AS08 Ground motion Prediction Equations Based on the NGA-West2 Data Set*, PEER Report No. 2013/04, Pacific Earthquake Engineering Research Center, University of California, Berkeley, CA, 143 pp.
- Abrahamson, N. A., Silva, W. J., and Kamai, R., 2014. Summary of the ASK14 ground motion relation for active crustal regions, *Earthquake Spectra* **30**, 1025–1055.
- Abrahamson, N. A., and Somerville, P. G., 1996. Effects of the hanging wall and footwall on ground motions recorded during the Northridge earthquake, *Bulletin of the Seismological Society of America* **86**, S93–S99.
- Ancheta, T. D., Darragh, R. B., Stewart, J. P., Seyhan, E., Silva, W. J., Chiou, B. S.-J., Wooddell, K. E., Graves, R. W., Kottke, A. R., Boore, D. M., Kishida, T., and Donahue, J. L., 2013. *PEER NGA-West2 Database*, PEER Report No. 2013/03, Pacific Earthquake Engineering Research Center, University of California, Berkeley, CA, 134 pp.
- Boore, D., and Atkinson, G., 2008. Ground motion prediction equations for the average horizontal component of PGA, PGV, and 5%-Damped PSA at spectral periods between 0.01 s and 10.0 s, *Earthquake Spectra* **24**, 99–138.
- Boore, D. M., Stewart, J. P., Seyhan, E., and Atkinson, G. A., 2013. *NGA-West2 Equations for Predicting Response Spectral Accelerations for Shallow Crustal Earthquakes*, PEER Report No. 2013/05, Pacific Earthquake Engineering Research Center, University of California, Berkeley, CA, 134 pp.
- Boore, D. M., Stewart, J. P., Seyhan, E., and Atkinson, G. A., 2014. NGA-West2 equations for predicting PGA, PGV, and 5% damped PSA for shallow crustal earthquakes, *Earthquake Spectra* **30**, 1057–1085.
- Bozorgnia, Y., Abrahamson, N. A., Al Atik, L., Ancheta, T. D., Atkinson, G. M., Baker, J. W., Baltay, A., Boore, D. M., Campbell, K. W., Chiou, B. S.-J., Darragh, R., Day, S., Donahue, J., Graves, R. W., Gregor, N., Hanks, T., Idriss, I. M., Kamai, R., Kishida, T., Kottke, A., Mahin, S. A., Rezaeian, S., Rowshandel, B., Seyhan, E., Shahi, S., Shantz, T., Silva, W., Spudich, P., Stewart, J. P., Watson-Lamprey, J., Wooddell, K., and Youngs, R., 2014. NGA-West2 research project, *Earthquake Spectra* **30**, 973–987.
- Campbell, K. W., and Bozorgnia, Y., 2008. NGA ground motion model for the geometric mean horizontal component of PGA, PGV, PGD and 5% damped linear-elastic response spectra for periods ranging from 0.01 and 10.0 s, *Earthquake Spectra* **24**, 139–171.
- Campbell, K. W., and Bozorgnia, Y., 2013. *NGA-West2 Campbell-Bozorgnia Ground Motion Model for the Horizontal Components of PGA, PGV, and 5%-Damped Elastic Pseudo-Acceleration Response Spectra for Periods Ranging from 0.01 to 10 s*, PEER Report No. 2013/06, Pacific Earthquake Engineering Research Center, University of California, Berkeley, CA, 238 pp.

- Campbell, K. W., and Bozorgnia, Y., 2014. NGA-West2 ground motion model for the average horizontal components of PGA, PGV, and 5% damped linear acceleration response spectra, *Earthquake Spectra* **30**, 1087–1115.
- Chiou, B. S.-J., and Youngs, R., 2008. An NGA model for the average horizontal component of peak ground motion and response spectra, *Earthquake Spectra* **24**, 173–216.
- Chiou, B. S.-J., and Youngs, R. R., 2013. *Update of the Chiou and Youngs NGA Ground Motion Model for Average Horizontal Component of Peak Ground Motion and Response Spectra*, PEER Report No. 2013/07, Pacific Earthquake Engineering Research Center, University of California, Berkeley, CA, 76 pp.
- Chiou, B. S.-J., and Youngs, R. R., 2014. Update of the Chiou and Youngs NGA model for the average horizontal component of peak ground motion and response spectra, *Earthquake Spectra* **30**, 1117–1153.
- Donahue, J., and Abrahamson, N., 2013. *Hanging wall Scaling Using Finite-Fault Simulations*, PEER Report 2013/13, Pacific Earthquake Engineering Research Center, University of California, Berkeley, CA.
- Dreger, D. S., Beroza, G. C., Day, S. M., Goulet, C. A., Jordan, T. H., Spudich, P. A., and Stewart, J. P., 2013. *Evaluation of SCEC Broadband Platform Phase I Ground Motion Simulation Results*, Southern California Earthquake Center Report, 1 August 2013, Los Angeles, CA, 33 pp.
- Graves, R., and Pitarka, A., 2010. Broadband ground motion simulation using hybrid approach, *Bulletin of Seismological Society of America* **100**, 2095–2123.
- Idriss, I., 2008. An NGA empirical model for estimating the horizontal spectral values generated by shallow crustal earthquakes, *Earthquake Spectra*, **24**, 217–242.
- Idriss, I. M., 2013. *NGA-West2 Model for Estimating Average Horizontal Values of Pseudo-Absolute Spectral Accelerations Generated by Crustal Earthquakes*, PEER Report No. 2013/08, Pacific Earthquake Engineering Research Center, University of California, Berkeley, CA, 31 pp.
- Idriss, I. M., 2014. An NGA-West2 empirical model for estimating the horizontal spectral values generated by shallow crustal earthquakes, *Earthquake Spectra* **30**, 1155–1177.
- Pacific Earthquake Engineering Research Center (PEER), 2008. *Next Generation Attenuation of Ground Motions (NGA) Project*, University of California, Berkeley, CA.

(Received 19 July 2013; accepted 26 May 2014)